

Article

# Adsorption of N<sub>2</sub>, NO<sub>2</sub> and CO<sub>2</sub> on Epistilbite Natural Zeolite from Jalisco, Mexico after Acid Treatment

Miguel Angel Hernández-Espinosa <sup>1,\*</sup>, Karla Quiroz-Estrada <sup>2,\*</sup>, Vitalii Petranovskii <sup>3</sup>, Fernando Rojas <sup>4</sup> , Roberto Portillo <sup>5</sup>, Martha Alicia Salgado <sup>5</sup>, Miguel Marcelo <sup>6</sup>, Efraín Rubio <sup>7</sup> and Carlos Felipe <sup>8</sup>

<sup>1</sup> Departamento de Investigación en Zeolitas, Universidad Autónoma de Puebla, Puebla 72570, Mexico

<sup>2</sup> Doctorado en Nanociencias y Micro-Nanotecnologías,UPIBI, Instituto Politécnico Nacional, Ciudad de México 07340, Mexico

<sup>3</sup> Centro de Nanociencias y Nanotecnología, Universidad Autónoma de México, Carretera Tijuana-Ensenada, Km. 107, Ensenada 22860, Mexico; vitalii@cyn.unam.mx

<sup>4</sup> Departamento de Química, Universidad Autónoma Metropolitana, Iztapalapa, Ciudad de México 09340, Mexico; fernando@xanum.uam.mx

<sup>5</sup> Facultad de Química, Universidad Autónoma de Puebla, Puebla 72570, Mexico; portilloreyes@yahoo.com (R.P.); malicia.64@hotmail.com (M.A.S.)

<sup>6</sup> Facultad de Ingeniería Química, Universidad Autónoma de Puebla, Puebla 72570, Mexico; lifad8mike@gmail.com

<sup>7</sup> Centro Universitario de Vinculación y Transferencia de Tecnología, Universidad Autónoma de Puebla, Puebla 72570, Mexico; efrainrubio@yahoo.com

<sup>8</sup> Departamento de Biociencias e Ingeniería, CIEMAD, Instituto Politécnico Nacional, Ciudad de México 07340, Mexico; cfelipe@ipn.mx

\* Correspondence: vaga1957@gmail.com (M.A.H.-E.); k.quiroz.estrada@gmail.com (K.Q.-E.); Tel.: +54-222-229-5500 (ext. 7270) (M.A.H.-E.)

Received: 15 February 2018; Accepted: 4 May 2018; Published: 5 May 2018



**Abstract:** Emissions of carbon dioxide (CO<sub>2</sub>) and nitrogen dioxide (NO<sub>2</sub>) in recent years has been increased considerably. One way to reduce the concentration of these greenhouse gases in the atmosphere is adsorptive capture. This paper describes the main results of adsorption of N<sub>2</sub>, NO<sub>2</sub>, and CO<sub>2</sub> on epistilbite, both natural and on samples that were chemically treated at various concentrations of HCl. Data on the adsorption of CO<sub>2</sub> and NO<sub>2</sub> were evaluated by the Freundlich and Langmuir equations. Additionally, the thermodynamic parameters of adsorption were calculated, including the degree of interaction of the zeolite samples with gases by gradually changing the isosteric heat capacities of adsorption. The acid treatment improves the adsorption capacity of epistilbite with respect to NO<sub>2</sub> and CO<sub>2</sub>, due the replacement of large extra-framework cation by small H<sup>+</sup> ions. The improvement in the distribution of pore sizes in epistilbite samples was calculated by the method of Barrett-Joyner-Halenda. The sample H1 that was prepared in a moderately concentrated acid showed the best behavior in the CO<sub>2</sub> adsorption processes, while the natural EPIN material preferably adsorbs NO<sub>2</sub>.

**Keywords:** sequestration; carbon dioxide; epistilbite; adsorption

## 1. Introduction

Due to their unique properties, zeolites are widely used in industry, the Structure Commission [1] of the International Zeolite Association (IZA) [2] assigns 225 framework type codes (consisting of three capital letters) to all unique and confirmed framework topologies of natural and synthetic zeolites. Only 67 of them can be found in the nature [3], so, for them, both synthetic and natural moieties can

be found. It is well known that natural zeolites are cheap, but they have a variable composition and contain impurities, whereas synthetic zeolites are pure substances, but are expensive ones. Thus, when choosing a certain type of zeolite for practical application, it is necessary to decide how to minimize costs, but in such a way as to get the maximum effect. Synthetic and natural zeolites are commercially employed in view of their unique properties, such as ion-exchange, adsorption, molecular sieve, and catalytic activity, which are directly related to the properties of zeolite frameworks [4,5]. An incentive to choose a particular type of natural zeolite can be their really useful properties, and the fact that they are quite common in deposits. The most common natural zeolites are natrolite (NAT), analcime (ANA), chabazite (CHA), clinoptilolite (CLI), phillipsite (PHI), and stilbite (STI) [6]. Nevertheless, in recent years, geologists have discovered new significant sedimentary sources of zeolites all over the world. That is why we select natural epistilbite (IZA type code EPI) for this study.

There are many types of zeolites around the world, natural and synthetic; these materials are classified according with the number of tetrahedral members in the rings, forming their channels. Those in which the pores are formed from eight tetrahedral units are named as small pore zeolites, whilst if they have 10 member rings, these are called medium pore zeolites, in the case of 12 members, they are large pore zeolites (12-membered rings), and, finally, those presenting more than 12 members in tetrahedral coordination are defined like extra-large pore zeolites. Another way of classifying zeolites is related to the number of channel directions in zeolite crystals; if the zeolite channels are in one, two, or three different directions, then, such zeolites themselves are classified as one-dimensional, two-dimensional, or three-dimensional, respectively [7]. So, between the most abundant Mexican natural zeolites, ERI represents three-dimensional small pores one, with pore architecture of  $8 \times 8 \times 8$  members, while HEU belongs to medium pore zeolites with two-dimensional  $10 \times 8$  channel system, and MOR is a one-dimensional large pore zeolite with 12-membered rings [1]. Small pores adsorbents, like zeolites, are especially attractive for CO<sub>2</sub> capture at large emission sources, which could take advantage to reduce the energy demands in carbon dioxide separation processes from flue gas comparing with current technologies [8]. For this purpose, small pore zeolites are of great interest, inasmuch as the CO<sub>2</sub> kinetic diameter is smaller than N<sub>2</sub> and all most gasses, benefiting their entry in this porous solid. It is expected that small-pore zeolites will have an increased selectivity towards CO<sub>2</sub> [9].

From this point of view, epistilbite (EPI), belonging to small pore zeolites, is an important candidate because it has a two-dimensional  $8 \times 8$  pore architecture [1]. This zeolite possesses a system of channels with pore openings with dimensions of 0.37 nm  $\times$  0.45 nm and 0.36 nm  $\times$  0.36 nm in [001] and [101] directions, respectively, see Figure 1. Maximum diameter of a sphere that can be included in the EPI voids is 0.547 nm; diameters of the spheres that can diffuse along the channels in the [100] and [101] directions are 0.362 nm and 0.348 nm, correspondingly. Accessible volume is equal to 9.04% [1]. Accessible area, calculated from the idealized framework model, is equal to 1058.21 m<sup>2</sup>/g [1,10]. The chemical composition of this alkaline-earth zeolite is (Ca, Na<sub>2</sub>)<sub>3</sub>(Al<sub>6</sub>Si<sub>18</sub>O<sub>48</sub>)·16H<sub>2</sub>O [3] with a Si/Al atomic ratio close to 3 [1,3]. Breck [11] reported about a possible change of this ratio in the range from 2.58 to 3.02, but the degree of confidence to the early analyses is unknown.

The EPI datasheet [3] reports the variation of compositional range from 18.5 to 17.5 Si per unit cell. Dominant cation for EPI zeolite is always Ca<sup>2+</sup>, it comprises 65% to 90% of the non-framework cations; Ba<sup>2+</sup> and K<sup>+</sup> are minor components in all the analyses [3]. Epistilbite is poorly studied zeolite. Number of patents is registered, which proposed the epistilbite use. It may serve as de-NO<sub>x</sub> catalyst that provides superior NO control performance without substantial changing or affecting the hydrocarbon conversion during the FCC process [12,13], or functionalized silicate nanoparticles to remove the asphaltene particles [14]. This zeolite, among others, is recommended as activating additive in the cleaning liquid [15]. The data about upper thermal stability limit of epistilbite are controversial. Breck [11] reported that it is stable under vacuum till 250 °C. The synchrotron powder diffraction study of thermal dehydration process of the epistilbite from Osilo (Sardinia, Italy) showed that the upper stability limit is 515 °C [16]. Such value makes the practical use of EPI zeolite quite possible.

In this article, for the first time are reported physico-chemical characterization and study of CO<sub>2</sub> and NO<sub>2</sub> adsorption on epistilbite, with the aim of evaluating it as a possible friendly environment natural material for the separation of low molecular weight gases, having a greenhouse effect.

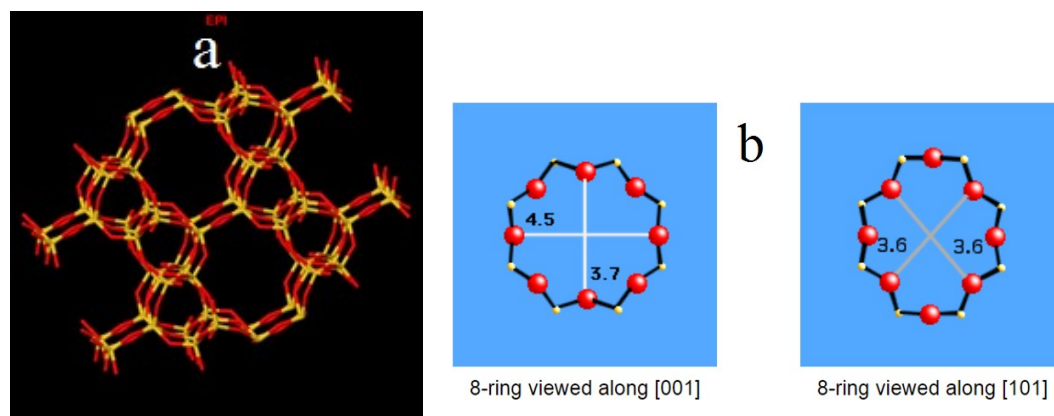


**Figure 1.** Epistilbite (EPI) (a) Framework and (b) Dimensions of eight member rings.

## 2. Materials and Methods

The samples of natural epistilbite that were studied in this work were obtained from the deposit in Zapopan, Jalisco, Mexico. A zeolitic rock was milled, and fraction with mesh 60–80 (diameter in the range of +150–250  $\mu\text{m}$ ) was selected for the experimental work. This natural sample was labelled as EPIN. Dealuminated epistilbite samples were prepared by an acid-leaching treatment; this process caused the exchange of polyvalent cations by protons, and the removal of framework aluminum and mineral impurities [17]. EPIN samples were subjected to the treatment in 0.01 N and 1.0 N solutions of hydrochloric acid and were tagged as EPIH1 and EPIH2, respectively. The acid treatment includes several cycles of contact with granular sample for 6 h at room temperature. Subsequently, epistilbite samples were washed with deionized water until negative test on Cl<sup>-</sup> anion with AgNO<sub>3</sub>.

### 2.1. Characterization

The X-ray powder diffraction pattern of the EPIN sample was collected at a variable temperature in the range of 2 $\theta$ : 5°–70°, using Bruker D8 DISCOVERED diffractometer, which employ a nickel filtered Cu K $\alpha$  radiation ( $\lambda = 0.154$  nm). X-ray Fluorescence (XRF) Analysis was done with Bruker XRF Spectrometer that was equipped with 3001 XFLHAS detector, with excitation and detection angles of 45°, using ARTAX software. Scanning Electron Microscopy images were obtained from a JEOL JSM-5300 electron microscope (JEOL Ltd., Mexico City, Mexico). To determine the textural properties of natural and dealuminated samples, high resolution N<sub>2</sub> adsorption isotherms were measured at the boiling point of liquid N<sub>2</sub> (76.4 K at the 2200 m altitude of Puebla City, Mexico) in an automatic volumetric adsorption system (Quantachrome AutoSorb-1C, Quantachrome Instruments, Boynton Beach, FL, USA). N<sub>2</sub> and He ultrahigh purity gases (>99.999%, INFRA Corp., Mexico City, Mexico) were employed. Before sorption experiments, epistilbite samples were outgassed at 623 K during 20 h at a pressure under 10<sup>-6</sup> mbar. The collected Isotherms were carried out in the range of relative pressure  $p/p^0$  [10<sup>-5</sup>–0.995].

### 2.2. CO<sub>2</sub> and NO<sub>2</sub> Adsorption

CO<sub>2</sub> and NO<sub>2</sub> adsorption isotherms were carried out on a gas chromatograph Gow-Mac 350 (GOW-MAC Instrument Co., Bethlehem, PA, USA), coupled with a thermal conductivity detector. The used chromatographic columns were of stainless steel with an internal diameter of 5 mm and a length of 50 cm. These columns were packed with zeolite sample (1–2 g) that was sieved with a

0.250 mm mesh sizes, which were outgassed with helium as the carrier gas at 573 K before adsorption experiments. NO<sub>2</sub> and CO<sub>2</sub> gases were injected using a 2 mL loop to introduce volume into the column, and finally to measure the retention times. The adsorption isotherms of the gas on the zeolites were determined at the temperature range of 423–573 K. The method of maximum chromatographic peaks [18]. (GC peak maxima method) provides a measure of the gas adsorbed amount using He (30 cm<sup>3</sup>·min<sup>-1</sup>) as carrier gas. Data corresponding to the adsorption of these gases on epistilbite samples were fitted, according to the mathematical models of Freundlich and Langmuir adsorption. Standard adsorption energies ( $-\Delta U_0$ ) and isosteric heat of adsorption at low degrees of coverage were calculated from the experimental adsorption isotherm data using Van't Hoff and Clausius-Clapeyron type equations. In order to perform the calculation of the adsorption equilibrium of the mixture (CO<sub>2</sub> and NO<sub>2</sub>) from the adsorption isotherms of the individual components, the approximate method of Lewis, Equation (1) [11] was applied. This method consists of representing a fraction of the total adsorption amount of each of the components, according to the molar fraction of component:

$$\left[ \frac{x_1}{a_1^0} + \frac{1-x_1}{a_2^0} \right] = \frac{1}{a_{12}^0} \quad (1)$$

where  $x_1$  and  $x_2$  are the mole fractions of the components in the adsorption phase that was calculated from GC measurements,  $a_1^0$  and  $a_2^0$  are the adsorption capacities of each component at a certain pressure constants  $P_1$  and  $P_2$ . For certain arbitrary values of  $x$ , there are a 12 values at each of the isotherm points of the pure components, and then the partial pressures  $P_1$  and  $P_2$  are calculated on the basis of the equilibrium isotherms. The molar ( $y_1$ ) and ( $y_2$ ) fractions in the gas phase are given by Equation (2):

$$y_1 = \frac{P_1}{P_1 + P_2}; y_2 = \frac{P_2}{P_1 + P_2} \quad (2)$$

A good indication of the ability for separation in an equilibrium based separation process is given by the adsorption selectivity  $Kp$  of the material for different gas species in the mixtures. The adsorption selectivity  $Kp$  of component 1 from component 2 was calculated as:

$$Kp = \frac{x_1 y_2}{x_2 y_1} \quad (3)$$

Another method for predicting the behavior of the adsorption of gas mixtures from the adsorption of pure gas, is to find the parameters of the separation coefficient  $\alpha_1$ , as determined by Equation (4):

$$\alpha_1 = \frac{K_{H1}}{K_{H2}} \quad (4)$$

where  $K_{H1}$  and  $K_{H2}$  are Henry constants of adsorbed gas in high and low levels, respectively.

### 3. Results and Discussion

#### 3.1. Morphology, Chemical Composition and X-ray Diffraction

The X-ray powder diffractogram of the EPI samples is shown in Figure 2a. The diffraction pattern indicates that in these tuffs epistilbite is combined with a certain amount of clinoptilolite. This figure shows the most characteristic peaks of crystalline epistilbite appear at the following diffraction angles:  $2\theta$ : 9.97°, 22.96°, 25.85°, 29.96°, 39.99°, 47.72°, 60.0° [19] and for clinoptilolite these are  $2\theta$ : 9.85°, 11.08°, 13.03°, 14.84°, 16.86°, 17.02°, 19.04°, 20.73°, 22.35°, 23.88°, 25.42°, 26.24°, 27.00°, 28.09°, 30.01°, 32.31°, 32.57°, and 34.80°.

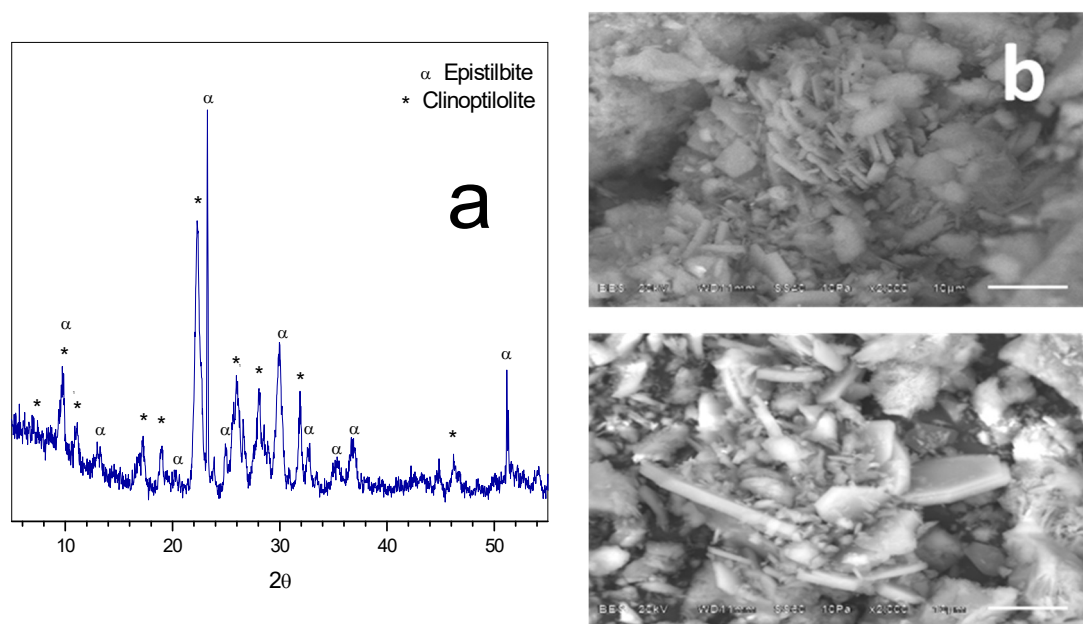


**Figure 2.** (a) XRD pattern of natural zeolite epistilbite; and, (b) SEM images of epistilbite zeolite fibres.

Figure 2b displays SEM micrographs that reveal the microstructures that were attained by epistilbite samples, either natural or chemically treated with HCl solutions. Analysis of scanning electron microscopy, performed with epistilbite zeolites, showed aggregates of thin crystals in semicubic forms with different geometries and varying sizes of about 1–5 microns.

The results of XRF analysis of chemical compositions of all the epistilbite substrates are listed in Table 1. This Table shows the decrease in the percentage of aluminum that is related to the change in the concentration of cations that are present in the samples that were chemically treated with washing in HCl. Another interesting fact is the presence of Zr and Ti in the EPIN which comes from the same impurities of its origin and they are eliminated in its entirety in the sample EPIH2.

**Table 1.** Chemical XRF elemental analyses of epistilbite zeolites (wt %).

Element	EPIN	EPIH1	EPIH2
Si	66.374	68.361	69.103
Al	1.837	1.246	1.263
Fe	21.786	19.907	21.473
Ca	1.816	2.745	2.098
Sr	2.973	0.426	0.7045
K	1.765	1.545	1.855
Rb	1.248	1.222	1.647
Y	Nd	1.222	Nd
Ni	Nd	0.596	Nd
Cu	0.292	0.426	1.020
Zn	Nd	0.427	0.785
Ti	0.345	Nd	Nd
V	Nd	0.796	Nd
As	Nd	Nd	Nd
Zr	1.558	2.580	Nd
Cl	0.001	0.001	0.007
<b>Total %</b>	<b>99.995</b>	<b>99.955</b>	<b>99.955</b>

Nd: not detected.

### 3.2. N<sub>2</sub> Adsorption

N<sub>2</sub> adsorption isotherms at 77 K on EPIN and EPIH zeolites are shown in Figure 3a. This figure describes the evolution of the shapes of N<sub>2</sub> isotherms with respect to the number of HCl washings; the EPIN and EPIH substrates render IUPAC type IV isotherms (with extremely narrow hysteresis loops), while a type I isotherm is proper for the EPIH2 specimen (the hysteresis loop of this sample corresponds to a IUPAC type H4) [20]. Distinctive features of these types of isotherms are as follows. First of all, the extent of microporosity in dealuminated epistilbites as a whole increase with the number of acid treatments, then, the plateaus of the N<sub>2</sub> isotherms corresponding to EPIH epistilbites reach increasing heights, in accordance with the accessible microporosity that is inherent in each zeolite; and, finally, the existence of a low-pressure hysteresis region is evident for the EPIH2 specimen. It is also important to note that EPIH2 possesses a microporous volume that is several times larger than that of EPIN. Therefore, acid treatment of high-silica natural epistilbite can render adsorbents of enhanced accessible pore volumes via the mechanism of decationation and dealumination, and by the dissolution of any amorphous materials blocking the entrances to the channels of the epistilbite structure. The cation blocking effects at pore entrances in natural epistilbites are diminished by acid treatment, then decreasing the availability of active cation exchange sites of the resultant substrates by leaching out Al<sup>3+</sup> from framework positions and introducing H<sup>+</sup> into the remaining cation sites of the natural precursor.

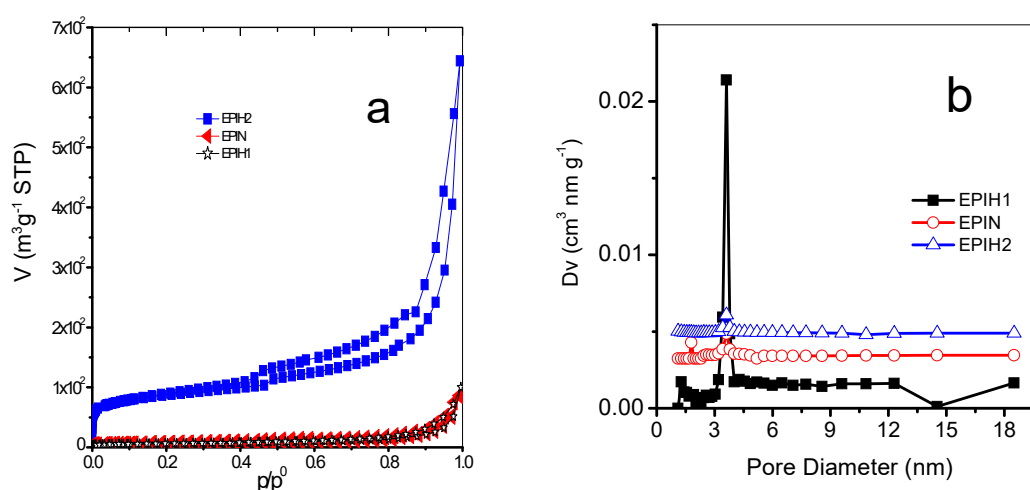


**Figure 3.** (a) N<sub>2</sub> adsorption isotherms at 77 K on epistilbite zeolites and (b) Pore size distributions (PSD) of exchanged epistilbite zeolites calculated from Barrett-Joyner-Halenda (BJH) method.

The isotherms of the EPI zeolites (Figure 3a) shows an upward deviation at high relative pressures due to the multilayer formation and capillary condensation taking place in the mesopores (secondary porosity) of this sample. Figure 3b shows the curves calculated by the Barrett-Joyner-Halenda (BJH) method. In this figure, EPIN and EPIH zeolites exhibits a sharp unimodal distribution with pore size maxima happening at 3.6 nm. However, intensity distribution for EPIH1 zeolite is greater with respect to EPIH2 and EPIN. The existence of a low-hysteresis loop that is associated with this substrate can mean that microporous channels are either interconnected to each other by thin capillaries or are surrounded by narrow cracks that are due to the dealumination process. The EPIH1 solid represents a transitional substrate with porous characteristics between those of the EPIN and EPIH2 structures.

Important textural properties ( $A_{SB}$ , BET specific surface area;  $C_B$ , BET constant;  $A_{SL}$ , Langmuir specific surface area;  $A_{St}$ , t-plot surface area;  $V_{\Sigma}$ , volume adsorbed at  $p/p^0 = 0.95$ ;  $D_p$ , particle diameter;  $\delta_r$ , real density; and,  $\epsilon$ , porosity.  $W_{0t}$  volume micropore estimated from t-plots of EPIN and EPIH epistilbites are listed in Table 2. For the EPIH2 epistilbite, the BET equation  $C_B$  constant is negative,

and this can be explained by the fact that multilayer adsorption in micropores is not a plausible model therein.

**Table 2.** Textural parameters of natural (EPIN) and ion-exchanged ( $H^+$ ) epistilbite zeolites, as determined from  $N_2$  adsorption.

Sample	$A_{SL}$ ( $m^2/g$ )	$A_{SB}$ ( $m^2/g$ )	$C_B$	$V_{\Sigma}$ ( $cm^3/g$ )	$W_{0t}$ ( $cm^3/g$ )	Dp (nm)	$\delta r$ ( $g/cm^3$ )	$\epsilon$ (%)
EPIN	45.48	62.69	111	0.0511	0.00184	30.6	1.39	0.0625
EPIH1	42.5	20.90	203	0.05631	0.00184	38.2	1.91	0.0368
EPIH2	415	306	−32	0.452	0.0424	58.8	1.74	0.0726

Textural parameters of the natural and dealuminated epistilbites adjust their behavior with the following order:  $A_{SL}$ : EPIH2 > EPIN > EPIH1, while  $V_{\Sigma}$ : EPIN > EPIH2 > EPIH1 and Finally,  $W_{0t}$ : EPIH2 > EPIH1  $\cong$  EPIN. There exists a concordance among performance of  $A_{SL}$  and  $W_{0t}$ , nevertheless  $V_{\Sigma}$  presents a highest value for a dealuminated epistilbite (EPIH2).

### 3.3. Adsorption of $CO_2$ and $NO_2$

Isotherms of  $CO_2$  and  $NO_2$  adsorption on epistilbite were measured at temperatures of 423, 473, 523, and 573 K by a gas chromatography (for details see Experimental section), Figures 4 and 5. Taking into account the behavior of the isotherms in Figure 6, it can be assumed that if a mixture of  $CO_2$  and  $NO_2$  will contact with the epistilbite, the adsorption phase will be enriched by  $CO_2$ , while gas phase by  $NO_2$ . The Lewis method (Equation (1)) and Langmuir model were used to determine the selectivity of adsorption  $K_p$  and separation coefficient  $\alpha$  (Equations (3) and (4)) in order to perform the calculation of the adsorption equilibrium. Parallel standard adsorption energies ( $-\Delta U_0$ ) were evaluated, whereas the isosteric heats of adsorption ( $-q_{st}$ ) were estimated according to the evolution of the degree of interaction of  $CO_2$  with the zeolite (Figure 6).

Mathematical adjustments of Freundlich and Langmuir [21] models were employed in order to analyze  $CO_2$  and  $NO_2$  isotherms data. The corresponding values of these models (Freundlich constants  $K_F$  and  $n$ , Henry constants  $K_H$ , Langmuir monolayer adsorption capacity  $a_m$ ) are given in Tables 3 and 4.

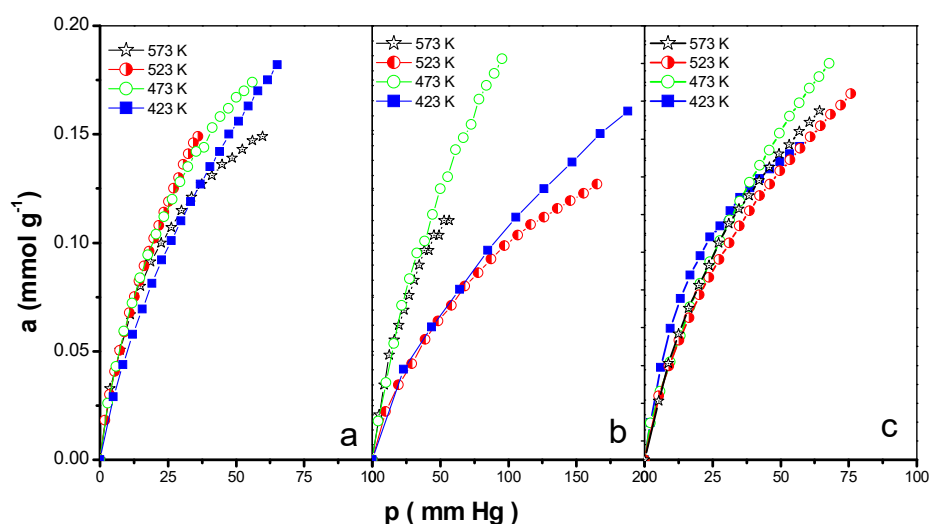


**Figure 4.** Adsorption isotherms of  $CO_2$  on: (a) EPIN, (b) EPIH1, and (c) EPIH2 zeolites.

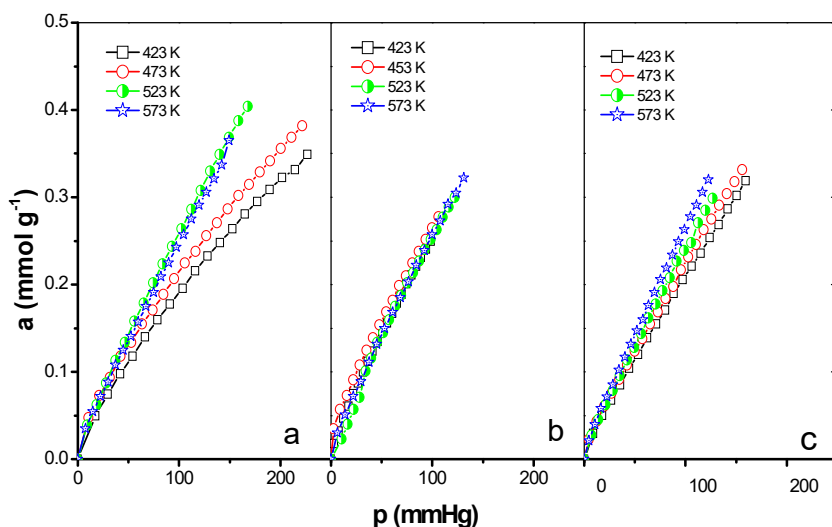


Figure 5. Adsorption isotherms of NO<sub>2</sub> on (a) EPIN, (b) EPIH1, and (c) EPIH2 zeolites.

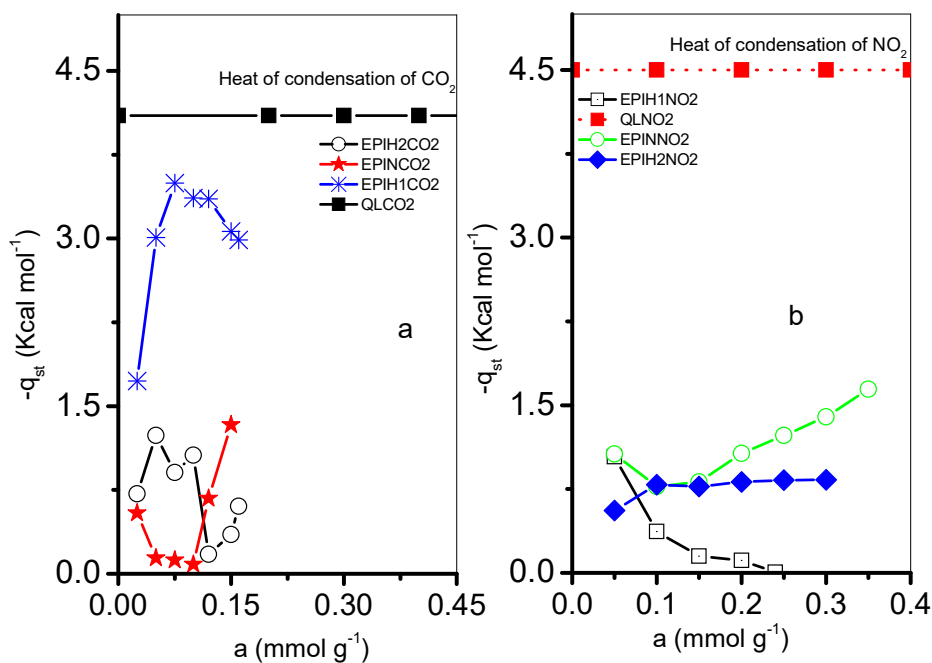


Figure 6. Variation of the isosteric heat of adsorption ( $-q_{st}$  Kcal·mol<sup>-1</sup>) of (a) CO<sub>2</sub> and (b) NO<sub>2</sub> with adsorbate loading on substrates.

Table 5 shows the selectivity of adsorption and separation coefficients of EPI zeolites for all gas mixtures that were considered in this study at 423, 473, 523, and 573 K. The initial increase in CO<sub>2</sub> selectivity is due to the strong electrostatic interactions between CO<sub>2</sub> molecules and EPI surface atoms at low loadings. At higher loadings, the packing effects come into play and smaller CO<sub>2</sub> molecules fit into the available channels, decreasing the adsorption selectivity toward CO<sub>2</sub>. EPIH2 shows significantly higher adsorption selectivity for CO<sub>2</sub> than widely studied EPIN zeolites under the same conditions. The selectivity found of CO<sub>2</sub> over NO<sub>2</sub> could be associated to the high thermodynamic interaction among the exchange cations Ca, Mg, and K and CO<sub>2</sub>. Additionally, EPIN is composed by narrower pores than EPIH zeolites, and therefore there is a stronger adsorption of CO<sub>2</sub> molecules [22].

**Table 3.** Henry, Freundlich and Langmuir parameters for the adsorption of CO<sub>2</sub> on EPIN and EPIH exchanged zeolites.

Sample	T (K)	$K_f \times 10^2$ (mmol·g <sup>-1</sup> ·mmHg <sup>-1</sup> )	<i>n</i>	<i>R<sub>F</sub></i>	<i>a<sub>m</sub></i> (mmol·g <sup>-1</sup> )	$K_H \times 10^3$ (mmol·g <sup>-1</sup> ·mmHg <sup>-1</sup> )	<i>R<sub>L</sub></i>
EPIN	423	1.8	0.539	0.993	0.183	8.9	0.996
	473	1.4	0.635	0.996	0.229	9.6	0.997
	523	1.0	0.705	0.999	0.281	6.3	0.998
	573	1.2	0.701	0.999	0.191	10.6	0.995
EPIH1	423	1.2	0.673	0.984	0.299	6.6	0.998
	473	0.9	0.750	0.999	0.459	5.9	0.999
	523	0.8	0.654	0.995	0.329	3.0	0.992
	573	0.8	0.621	0.999	0.224	3.6	0.992
EPIH2	423	1.6	0.611	0.991	0.238	9.9	0.999
	473	1.2	0.643	0.996	0.255	7.1	0.996
	523	1.1	0.681	0.999	0.311	6.7	0.999
	573	1.1	0.708	0.998	0.218	9.2	0.987

**Table 4.** Henry, Freundlich and Langmuir parameters for the adsorption of NO<sub>2</sub> on EPIN and EPIH exchanged zeolites.

Sample	T (K)	$K_f \times 10^2$ (mmol·g <sup>-1</sup> ·mmHg <sup>-1</sup> )	<i>n</i>	<i>R<sub>F</sub></i>	<i>a<sub>m</sub></i> (mmol·g <sup>-1</sup> )	$K_H \times 10^3$ (mmol·g <sup>-1</sup> ·mmHg <sup>-1</sup> )	<i>R<sub>L</sub></i>
EPIN	423	1.8	0.761	0.993	0.465	3.4	0.993
	473	1.4	0.699	0.996	0.305	5.0	0.984
	523	1.0	0.830	0.999	0.453	3.9	0.998
	573	1.2	0.799	0.999	0.419	3.9	0.993
EPIH1	423	1.2	0.761	0.999	0.239	6.2	0.982
	473	0.9	0.699	0.998	0.195	1.48	0.983
	523	0.8	0.830	0.998	0.843	2.2	0.994
	573	0.8	0.799	0.995	0.386	4.8	0.987
EPIH2	423	1.6	0.831	0.998	0.563	3.0	0.996
	473	1.2	0.782	0.995	0.414	4.6	0.984
	523	1.1	0.844	0.998	0.589	4.2	0.991
	573	1.1	0.841	0.998	0.414	4.7	0.987

**Table 5.** Selectivity of adsorption *K<sub>p</sub>* and separation coefficient  $\alpha_1$  of CO<sub>2</sub> and NO<sub>2</sub>, of EPI zeolites.

T (K)	<i>K<sub>p</sub></i>	$\alpha_1$
<b>EPIN</b>		
423	2.18	2.93
473	2.27	2.05
523	1.80	1.48
573	2.17	2.26
<b>EPIH1</b>		
423	1.98	1.06
473	1.52	2.48
523	1.49	1.36
573	2.00	1.34
<b>EPIH2</b>		
423	2.27	2.89
473	1.96	1.41
523	1.83	1.71
573	2.06	2.02

### 3.4. Isotheric Heat of Adsorption and Standard Adsorption Energies

The isotheric heat of adsorption at different adsorbate loadings was evaluated from the adsorption isotherm data (Figure 6) by means of the Clausius–Clapeyron equation. To determine this parameter, low concentrations of adsorbed gas are used in order to obtain the thermodynamic degree of adsorbate-adsorbent interaction [23]. The trends of the isotheric heat of adsorption ( $-q_{st}$ , Kcal/mol) as a function of the amount adsorbed of CO<sub>2</sub> and NO<sub>2</sub> adsorptive on EPIN and EPIH zeolites are presented in Figure 6.

## 4. Conclusions

The modified epistilbite zeolites with acid treatment produce modified materials that are capable of adsorbing greenhouse gases, as is the case of CO<sub>2</sub> and NO<sub>2</sub>. Large, blocking cations at pore entrances are substituted by protons with small ionic radius, then providing ready access to different greenhouse gases into the epistilbite channels; the concomitant modified of the structure that is brought by the exchanging treatment enhances channel widths. According to the BJH method, the PSD curves of the obtained epistilbite samples show an average pore diameter of about 3.5 nm; the results show that, according to the N<sub>2</sub> isotherm, the chemical treatment of these zeolites, especially in the EPIH2 sample, promotes the opening of the blocked microporosity by the exchange cations.

**Author Contributions:** M.A.H.-E. conceived and designed the experiments; R.P., E.R., M.A.S., C.F., M.M., and F.R. carried out the experiments; M.A.H.-E., K.Q.-E. and V.P. analyzed the data and wrote the paper.

**Conflicts of Interest:** The authors declare no conflict of interest.

## References

1. Database of Zeolite Structures. Available online: <http://www.iza-structure.org/databases/> (accessed on 13 May 2017).
2. International Zeolite Association (IZA). Available online: <http://www.iza-online.org/> (accessed on 14 May 2017).
3. Index of Natural Zeolites Datasheets. Available online: [http://www.iza-online.org/natural/IZA-NZ\\_Datasheets.htm](http://www.iza-online.org/natural/IZA-NZ_Datasheets.htm) (accessed on 13 May 2017).
4. Tiwari, A.; Titinchi, S. *Advanced Catalytic Materials*; Schivener Publishing: Wiley, NJ, USA, 2015; p. 472.
5. Yang, S.; Lach-hab, M.; Vaismal, L.; Blaisten-Barojas, E.; Li, X.; Karen, V. Framework-Type determination for zeolite structures in the inorganic crystal structure database. *J. Phys. Chem. Ref. Data* **2010**, *39*, 1–44. [[CrossRef](#)]
6. Perego, C.; Carati, A. Zeolites and zeolite-like materials in industrial catalysis. In *Zeolites: From Model Materials to Industrial Catalysts*; Cejka, J., Perez-Pariente, J., Roth, W.J., Eds.; Transworld Research Network: Kerala, India, 2008; pp. 357–389.
7. Moliner, M.; Martinez, C.; Corma, A. Synthesis strategies for preparing useful small pore zeolites and zeotypes for gas separations and catalysis. *Chem. Mater.* **2014**, *26*, 246–258. [[CrossRef](#)]
8. Weast, R.C. *CRC Handbook of Chemistry and Physics*, 95th ed.; CRC Press: New York, NY, USA, 2014.
9. Foster, M.D.; Rivin, I.; Treacy, M.M.J.; Delgado, F.O. A geometric solution to the Largest-Free-Sphere problem in zeolite frameworks. *Microporous Mesoporous Mater.* **2006**, *90*, 32–38. [[CrossRef](#)]
10. Cheung, O.; Hedin, N. Zeolites and related sorbents with narrow pores for CO<sub>2</sub> separation from flue gas. *RSC Adv.* **2014**, *4*, 14480–14494. [[CrossRef](#)]
11. Breck, D.W. *Zeolite Molecular Sieves*; Wiley-Interscience: New York, NY, USA, 1974; pp. 644–652.
12. Yaluris, G.; Zhao, X.; Ziebarth, M.S. Reducing Nitrogen Oxide Emissions Involves Incorporating a Nitrogen Oxide Reduction Zeolite Component with a Catalytically Cracking Catalyst Inventory That Is Being Circulated Throughout a Fluid Catalytic Cracking Unit. Patent No. US7641787-B2, 5 January 2010.
13. Tumsek, F.; Inel, O. Evaluation of the thermodynamic parameters for the adsorption of some *n*-alkanes on a type zeolite crystals by inverse gas chromatography. *Chem. Eng. J.* **2003**, *94*, 57–66. [[CrossRef](#)]

14. Khabashesku, V.; Mazyar, O.; Chakraborty, S.; Agrawal, G.; Hain, T. Functionalized Silicate Nanoparticle Composition, Removing and Exfoliating Asphaltenes with Same. Patent No. US9012377-B2, 31 December 2012.
15. Field, B.F. Apparatus for Cleaning a Surface Comprises A Mobile Body; First Liquid Line Configured to Receive a Liquid; a Container Coupled to the First Liquid Line; a Second Liquid Line Coupled to the Container; and Dispenser. Patent No. US2010276301-A1, 4 November 2010.
16. Cruciani, G.; Martucci, A.; Meneghini, C. Dehydration dynamics of epistilbite by in situ time resolved synchrotron powder diffraction. *Eur. J. Miner.* **2003**, *15*, 257–266. [[CrossRef](#)]
17. Hernández, M.A.; Portillo, R.; Salgado, M.A.; Rojas, F.; Petranovskii, V.; Salas, R.; Pérez, G. Comparación de la capacidad de adsorción de CO<sub>2</sub> en clinoptilolitas naturales y tratadas químicamente. *Superf. Vacío* **2010**, *23*, 67–72.
18. Choudary, V.R.; Mantri, K. Adsorption of aromatic hydrocarbons on highly siliceous MCM-41. *Langmuir* **2000**, *16*, 7031–7037. [[CrossRef](#)]
19. Treacy, M.; Higgins, J. *Collection of Simulated XRD Powder Patterns for Zeolites*; Elsevier: New York, NY, USA, 2001; pp. 49–50.
20. Thommes, M.; Kaneko, K.; Neimark, A.; Olivier, J.; Rodriguez, F.; Rouquerol, J.; Sing, K. Physisorption of gases, with special reference to the evaluation of surface area and pore size distribution (IUPAC Technical Report). *Pure Appl. Chem.* **2015**, *87*, 1051–1069. [[CrossRef](#)]
21. Atci, E.; Erucar, I.; Keskin, S. Adsorption and transport of CH<sub>4</sub>, CO<sub>2</sub>, H<sub>2</sub> mixtures in a bio-MOF material from molecular simulations. *J. Phys. Chem. C* **2011**, *115*, 6833–6840. [[CrossRef](#)]
22. Canet, X.; Nokerman, J.; Frere, M. Determination of the Henry constant for zeolite-VOC systems using massic and chromatographic adsorption data. *Adsorption* **2005**, *11*, 213–216. [[CrossRef](#)]
23. Hernández, M.A.; Asomoza, M.; Rojas, F.; Solís, S.; Salgado, M.A.; Portillo, R.; Jimenez, D. VOCs physisorption on micro-mesoporous solids: Application for dichloroethylene, trichloroethylene, and tetrachloroethylene on SiO<sub>2</sub> and Ag/SiO<sub>2</sub>. *J. Environ. Chem. Eng.* **2013**, 967–974. [[CrossRef](#)]



© 2018 by the authors. Licensee MDPI, Basel, Switzerland. This article is an open access article distributed under the terms and conditions of the Creative Commons Attribution (CC BY) license (<http://creativecommons.org/licenses/by/4.0/>).